A Density Functional Theory (DFT) Study on Gas-Phase Proton Transfer Reactions of Derivatized and Underivatized Peptide Ions Generated by Matrix-Assisted Laser Desorption Ionizatio...

ARTICLE *in* JOURNAL OF THE AMERICAN SOCIETY FOR MASS SPECTROMETRY · APRIL 2009

Impact Factor: 2.95 · DOI: 10.1016/j.jasms.2009.03.008 · Source: PubMed

A Density Functional Theory (DFT) Study on Gas-Phase Proton Transfer Reactions of Derivatized and Underivatized Peptide Ions Generated by Matrix-Assisted Laser Desorption Ionization

Francesco L. Brancia,[a] Mauro Stener,[b,c,d] and Alessandra Magistrato[d,e]

[a] Shimadzu Research Laboratory, Manchester, United Kingdom
[b] Dipartimento di Scienze Chimiche, Università di Trieste, Trieste, Italy
[c] Consorzio Interuniversitario Nazionale per la Scienza e Tecnologia dei Materiali (INSTM), Trieste, Italy
[d] CNR-INFM DEMOCRITOS National Simulation Center, Trieste, Italy
[e] SISSA/ISAS, Trieste, Italy

In this study, classic molecular dynamics (MD) simulations followed by density functional theory (DFT) calculations are employed to calculate the proton transfer reaction enthalpy shifts for native and derivatized peptide ions in the MALDI plume. First, absolute protonation and deprotonation enthalpies are calculated for native peptides (RPPGF and AFLDASR), the corresponding hexyl esters and three common matrices α-cyano-4-hydroxycinnamic acid (4HCCA), 2,5-dihydroxybenzoic acid (DHB), and 6 aza-2-thiothymine (ATT). From the proton exchange reaction calculations, protonation and deprotonation of the neutral peptides are thermodynamically favorable in the gas phase as long as the corresponding protonated/deprotonated matrix ions are present in the plume. Moreover, the gain in proton affinity shown by the ester ions suggests that the increase in ion yield is likely to be related to an easier proton transfer from the matrix to the peptide. (J Am Soc Mass Spectrom 2009, 20, 1327–1333) © 2009 Published by Elsevier Inc. on behalf of American Society for Mass Spectrometry

In UV matrix assisted laser desorption ionization (MALDI) mass spectrometry (MS) [1, 2], understanding of the factors determining the final appearance of a MALDI spectrum continues to be of interest to the scientific community. Current theories include a two-steps model in which differentiation between primary and secondary ionization processes relies on the time scale in which ions are formed [3–7]. In the first step (typically few nanoseconds), with the exception of preformed ions liberated in vacuum occurring in a much longer time scale [8], primary ions are generated in solid phase by laser irradiation. In the second step (microseconds) ion molecule reactions (secondary processes) occurring via multiple collisions between ions and neutrals take place in the expanding plume. Regardless of the type of processes involved, ions so generated are accelerated by the potential applied in the source till they reach the detector. Although the models describing primary processes are still under debate, the secondary processes occurring in the gas phase can be partially explained by conventional kinetics and thermodynamics [9].

Proton transfer is probably the most important type of secondary reactions observed in MALDI. Many analytes, especially peptides and proteins, are detected predominantly in protonated form. Reactions between peptides/proteins in the gas phase were reported to have proton affinities (PAs) greater than 215 kcal/mol [10], whereas PAs of the most common matrices are between 200 and 215 kcal/mol [11–13], making the proton transfer between protonated matrix and neutral analyte favorable. Strong evidence for proton transfer reactions between protonated matrix and analyte was recently reported using mixtures of conventional matrices and various amino acids varying in gas phase basicity [6]. In peptide analysis it was shown that the type of amino acid incorporated in the peptide backbone affects the abundance of the corresponding ions generated [14]. In particular, MALDI spectra of peptides derived from proteolytic digestion of proteins with trypsin indicated that the proton affinity of C-terminus amino acids governs the MALDI response of the resulting peptide ions and lysine containing peptides generated by tryptic digestion of proteins produce ions detected in lesser abundance than those incorporating arginine [15]. Modification of the chemical moieties may result in more basic preformed ions in the solid phase along with their higher reactivity in the

Address reprint requests to Dr. Francesco Brancia, Shimadzu Research Laboratory, Trafford Wharf Road, Wharfside, M17 1GP, Manchester, UK. E-mail: Francesco.Brancia@srlab.co.uk

1044-0305/09/$32.00
doi:10.1016/j.jasms.2009.03.008

Published online March 20, 2009
Received October 6, 2008
Revised March 6, 2009
Accepted March 7, 2009

plume. To improve the sensitivity of the MALDI analysis of peptide mixtures, conversion of the acidic/basic character of a peptide by chemical derivatization can have an effect on ion yield and on fragmentation efficiency [16, 17].

Recently, esterification was used to investigate how introduction of aliphatic chains varying in length can affect the MALDI response of ions analyzed in both polarity regimes. It was found that while derivatization of carboxylic groups tended to increase detection of the modified protonated ions, in negative mode modification of acidic character showed a deleterious effect on formation of deprotonated species [18]. The explanation proposed suggested a selective suppression of the anionic species in the processes occurring in the plume with concomitant increased formation of protonated species. Proton affinities have been mostly determined measuring the equilibrium constants for gas-phase proton transfer between two bases. In the last decade, introduction of computational chemistry based methods has provided an alternative way to determine accurately the proton affinities of single amino acids [19, 20] and sodium affinities of small organic molecules [21]. Thermochemical properties of various UV and IR matrices were evaluated by means of B3LYP density functional molecular orbital calculations [22]. Recently, the mechanism of matrix-to-analyte proton transfer between DHB and the VPL tripeptide was investigated by a combination of molecular dynamics (MD) simulations followed by density functional theory geometry optimization [23]. In this paper, we use a density functional theory method to calculate the relative energies of the gas-phase processes occurring after expansion in vacuo. The absolute protonation and deprotonation enthalpies of native and modified peptides are determined, considering that these neutral molecules react with the most common protonated matrices present in the gas phase.

Computational Approach

In this work, we have employed a combination of classic molecular dynamics (MD) and density functional theory (DFT) method [24] to calculate the proton affinities (PA) and the gas-phase acidities (GA) of the peptides and matrices under study. If the system considered (peptide or matrix) is designated by S, we take into account both processes:

$$SH^+ \rightarrow S + H^+, \Delta E_{elec}^{PA} = E(S) + E(H^+) - E(SH^+), \quad (1)$$

$$S \rightarrow (S - H^+)^- + H^+, \Delta E_{elec}^{GA} = E((S - H^+)^-) + E(H^+) - E(S)\cdot \quad (2)$$

The reaction energies of (1) and (2), designated by ΔE_{elec}^{PA} and ΔE_{elec}^{GA} respectively, correspond to variations of internal energy, and are calculated at the density functional theory (DFT) level as described later. PA values are calculated, and reported in the tables, as enthalpy changes at 298 K for both reactions (1) and (2), employing the following expression [22]:

$$PA_{298} = \Delta E_{elec}^{PA} + \Delta(PV) + \Delta(ZPE) + \Delta E_{vib(298)} + \Delta E_{rot(298)} + \Delta E_{trans(298)} \quad (3)$$

In expression (3), the five additive terms to transform electronic internal energy to enthalpy are, respectively, the Δ(PV) term equal to RT, the variation of the zero point energy (ZPE) correction, the vibrational, rotational, and translational corrections. An identical expression is employed for the GA as well. We have disregarded, for the sake of computational economy, the $\Delta(ZPE)$ and the $\Delta E_{vib(298)}$ terms, while employing a classic treatment of rotational and translational corrections, a null term is obtained for the rotational contribution and a 3/2RT contribution is obtained for the translational correction.

In this work, we consider two arginine-containing peptides, constituted of five (RPPGF) and seven amino acids (AFLDASR), respectively. Due to the large number of possible conformations that the peptides can assume, we initially perform a conformational search via classic MD. The AMBER parm99 force field is used [25, 26] for the classic MD simulations. For the amino acids for which we consider protonation states or esterified forms not available in the parm99 force field (i.e., N-terminal Arg negatively charged, N-terminal Arg in its neutral form, C-terminal Phe in its neutral form, *n*-hexyl ester of C-terminal Phe, C-terminal Arg in its neutral form (deprotonated on guanidine group and protonated on carboxylic group), C-terminal Arg positively charged, *n*-hexyl ester of C-terminal Arg in the neutral form, *n*-hexyl ester of C-terminal Arg; N-terminal Ala in its neutral form, *n*-hexyl ester of Asp) we have initially optimized the geometries at B3LYP 6-31G* level [27, 28] employing the Gaussian03 program (www.gaussian.com, Gaussian Inc., Wallingford, CT). RESP charges are obtained by performing single point calculations on the optimized geometries at the Hartree-Fock 6-31G* level according to the Merz-Kollman scheme [29, 30] using the RESP module [28] of the AMBER 9 program [25, 26]. The selected peptides are considered in their neutral, protonated, deprotonated forms, along with the corresponding hexyl esters (neutral and protonated). After an initial heating of the system from 0 to 500 K in 1.2 ns, 25 ns of MD are performed at 500 K with a time step of 2 fs. For each system, 5 snapshots (every 5 ns) are selected, and these structures are then quenched from 500 to 0 K in 2 ns, and subsequently minimized. Relative energies of the selected snapshots are given in the Supplementary Information, which can be found in the electronic version of this article. These differ by a minimal value of 1 kcal/mol up to 45 kcal/mol (Table S11 and S12). Potential energies for each of neutral, protonated, deprotonated forms, along with the corresponding hexyl esters derivative, aver-

aged over the 25 ns of MD trajectories, are also given in Table S11 and S12.

Each of the five snapshot structures previously optimized at the molecular dynamics level are also optimized at the DFT level as described in the following part without any geometrical constraint. Although we cannot be sure that a complete search of the conformational space has been carried out due to the limited length of our trajectories and due to the selection of five representative snapshots, the number of snapshots selected is hampered by the need of performing DFT calculations to establish which the most stable conformer is. In fact, relative classic and DFT energies are uncorrelated and a DFT minimization is required (vide infra) [31, 32].

To obtain both PA and GA, the energies of all reactants and products of reactions (1) and (2) are calculated by means of the ADF program [33, 34], which solves the DFT Kohn-Sham equations employing a basis set of Slater type orbitals (STO). In actual calculations, the energy of a specific species is calculated with respect to the reference of the neutral atoms. In the present calculations, the geometries of all the snapshots obtained from the previous MD calculations are optimized employing a double zeta polarized (DZP) STO basis set and the local density approximation [19] to the exchange-correlation energy functional according to the parameterization suggested by Vosko et al. [35]. Starting from all the MD snapshots, the structure with the lowest energy obtained after the DFT optimization is taken as the most stable conformer. On the latter, a single point calculation is performed with the Becke-Perdew generalized gradient approximation (BP GGA) exchange-correlation energy functional [27, 36], to obtain more accurate energies. As observed in similar studies, relative energies obtained from DFT calculations are totally uncorrelated with the relative classic energies. The optimized geometries of both peptides for the native and *n*-hexyl derivatized species, and for neutral, protonated and deprotonated terms, are reported in the Supporting Information, together with a figure for each structure. For both peptides, the protonation site is the guanidino moiety on arginine while the deprotonation site is the carboxylic group of the C terminus amino acid. For the matrices, different protonation sites are tested to determine always the most stable structure (vide infra). Finally, it must be emphasized that in the following discussion the protonation and deprotonation enthalpies are employed to assess the thermodynamics of the various processes, disregarding the entropic effects. However in the present context entropic effects should play only a minor role. In fact, according to Harrison [10] it is possible to split the entropic effects into translational, rotational, and vibrational contribution. Vibrational contribution is negligible at room temperature, while translational contribution is important when the number of reactants is different with respect to the number of products: this occurs for the reaction involving free protons (see eqs 1 and 2), but it does not happen for the matrix–peptide proton exchange reaction, which is the target of the present study. Therefore, our work should not be affected by translational entropic effects. On the other hand, it is known that the rotational entropic contribution may play a significant role when the protonation causes the formation of strong intramolecular hydrogen bonds, which can freeze one rotational degree of freedom. The magnitude of such rotational entropy should be around -20 cal mol^{-1} K^{-1} [10], therefore the Gibbs free-energy of the protonation reaction may differ by at most +6 kcal/mol with respect to the present calculations, and this will not alter the conclusions obtained in this study. In the presence of multiple hindered rotations and for temperature much higher than 298 K, as expected to occur inside the MALDI plume, the entropic effects might exceed 6 kcal/mol. However, the treatment of this phenomenon remains an open problem: to our knowledge, at the moment there are no theoretical models that can reliably address the entropic effects for peptides and MALDI matrices. From the experimental point of view, instead, measurements with temperature changes, like the extended kinetic method, can give access to quantitative estimates of protonation entropy [37].

Validation of the Computational Method

Since previous works use different computational approaches [22, 23], the present theoretical method needs to be validated first. The main reason to try the density functional theory (DFT) approach is the advantage that, in principle, this approach can have when large molecules containing more than 100 atoms are studied. However, it is important to point out that the present strategy is not considered as a universal method to calculate absolute PA and GA energies of large peptides, but rather an alternative approach to give a quantitative estimate of the shifts in PA between the derivatized and underivatized peptides.

In Table 1, the PAs obtained using DFT are listed for three different amino acids together with the results obtained using the previous DFT and MP2 methods [20]. We notice that with respect to these results the newly calculated PAs are overestimated at most by 4.9 kcal/mol for lysine. The discrepancies observed should be attributable to the different exchange correlation functional and basis set employed as well as to the fact that in the present work, the ZPE corrections are ignored. The ZPE corrections for the protonation, how-

Table 1. Proton affinities (PA) for selected amino acids calculated with the present DFT method, compared with previous results from reference [20]. The values are indicated in kcal/mol

	Present DFT	DFT [21]	MP2 [21]
Ala	219.1	215.0	215.2
Lys	242.2	237.3	237.1
Arg	255.0	253.3	250.2

ever, are largely constant; in fact, from reference [20], the differences between the ZPE for the protonated and the neutral forms span between 8.1 and 9.6 kcal/mol for all amino acids, so although they affect the absolute PA, when differences are considered, the ZPE corrections tend to cancel each others within an expected error of about 2 kcal/mol. Since the main goal of the present work is to identify the effect of *n*-hexyl esterification on the PA, we assume that such error is reasonably acceptable when the calculated PA differences are much larger than 2 kcal/mol, a condition that is safely verified for the peptides presently considered.

Results and Discussion

The first part of this study focuses on the calculation of the PAs of selected peptides protonated in the gas phase, which is the necessary step before the determination of the PA shifts between native and derivatized peptides. Although our method has not been designed for such purpose, we find it convenient to compare our calculated values with the experimental data. We do not expect quantitative matching, but rather we want to ascertain whether the results obtained are sound. Two peptides (RPPGF and AFLDASR) and their corresponding hexyl esters are used in this investigation. Although the size of the peptides examined is small compared with the average size of the peptides used in peptide mass fingerprint (PMF) type experiments, our choice is dictated by the time constraint for the calculations (the minimization of larger peptides would require more computational effort) and by the prior knowledge on the gas-phase behavior of these chemically modified peptides [16, 18, 38, 39].

As shown previously, esterification of the carboxylic groups induces an increase in MALDI response for the derivatized peptide ions [18]. If esterification has an impact directly on the ion/molecule reactions in gas phase, large variations in PAs are expected to be observed between peptides and their derivatized analogues. The calculated values of PA and GA (eqs 1 and 2) are reported in Table 2. The PAs range between 259 and 279 kcal/mol, showing that these ab initio calculations are consistent with the proton affinities measured experimentally for peptides and proteins (in the order of 240 kcal/mol) [10]. Figure 1 illustrates the most energetically stable neutral specie of RPPGF for its native form (a) and for its hexyl ester (b). It is generally assumed that the hexyl esterification should favor protonation, due to the electron donor property of the alkyl

Table 2. Proton affinity (PA) and gas-phase basicity (GA) for RPPGF, AFLDASR, and their corresponding esters (kcal/mol)

Peptide	PA	GA
RPPGF	259	327
Hexyl RPPGF	270	—
AFLDASR	266	307
Hexyl AFLDASR	279	—

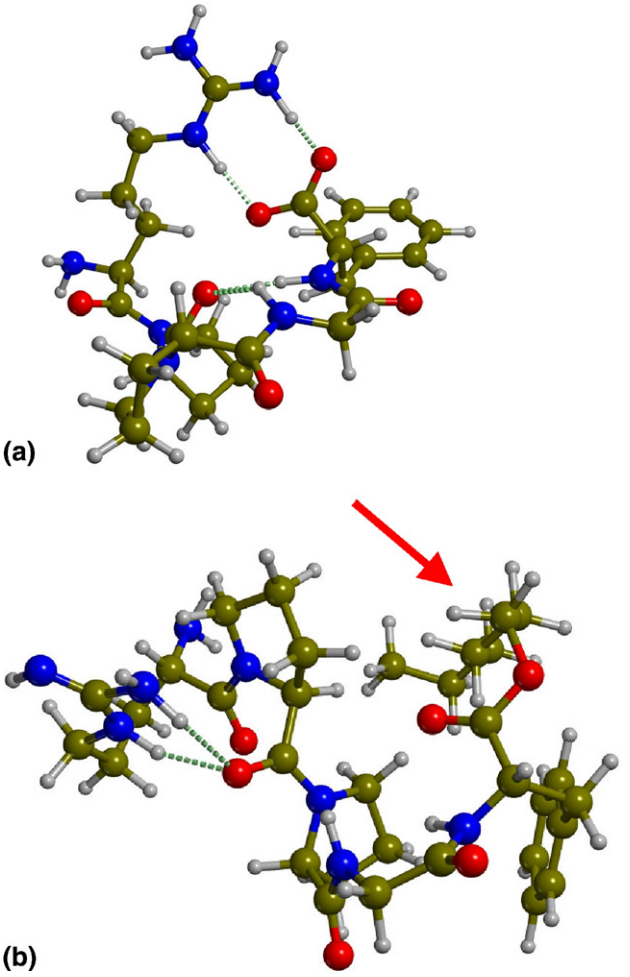

Figure 1. The energetically most stable species of RPPGF in its underivatized form (**a**), with its hexyl ester (**b**). The arrow indicates the position of the hexyl group.

group, the calculations show that the hexyl esterification has an important effect on the PAs, resulting in a stabilization of 11 kcal/mol for the hexyl ester of RPPGF and a stabilization of 13 kcal/mol for hexyl AFLDASR. The structures reported in Figure 1 may suggest a more convincing explanation of how derivatization influences gas-phase basicity: in the hexyl derivative of the peptide the hydrogen bonds are formed with more difficulty with respect to the native counterpart due to the steric hindrance of the bulky and hydrophobic alkyl chain. Moreover, in the native neutral peptides (see also Figures S1 and S6 of the Supporting Information) a salt bridge is present, between the guanidinium group of the arginine residue and, respectively, the C-terminal carboxylic acid for RPPGF and the aspartic acid carboxylate for AFLDASR. Such salt bridge represents a further stabilization factor for the neutral peptides, which cannot be found in the derivatized forms due to the hexylation of the carboxylate groups [31, 42]. To assess the strength of the salt bridge observed in both peptides, we have verified its presence in all DFT optimized structures. For RPPGF all opti-

mized structures lie within 2 kcal/mol with respect to the most stable structure. Conversely, for AFLDASR the optimized structure without salt bridge is less stable by 17 kcal/mol with respect to the most stable structure, a value which may represent an estimate of the contribution of the salt-bridge formation in the stabilization of the neutral form.

Since the esterified carboxylic group is less involved in the formation of hydrogen bonds, the neutral derivative is less stabilized and salt bridge formation is not observed. On the other hand, in the protonated form the hydrogen bonds are less influenced by derivatization. Since the esterification destabilizes the neutral form upon protonation a larger energy difference is obtained comparing the neutral with the protonated form so that a higher gas-phase basicity is obtained. These effects can be better appreciated comparing the figures of the different forms of the two peptides reported in the Supporting Information. The large increase in ion signal displayed by the protonated ester ions seems to indicate that the improved ability of the esterified peptide to be protonated during MALDI analysis is more related to the role played by the increase in proton affinity obtained by derivatization rather than to higher hydrophobicity of the added alkyl group, which facilitates incorporation of the peptide into the matrix crystal. In Table 2, the GAs are also displayed: large positive values (above 300 kcal/mol) are obtained in accordance with the expected difficulty to abstract a proton from the peptide carboxylic moieties.

Formation of peptide ions is expected also to occur via proton transfer between the protonated matrix ions present in large excess in the plume and the neutral macromolecules desorbed. In Table 3, PAs and GAs for the three matrices, DHB, ATT, and 4HCCA, are listed. For all three matrices, the choice of the protonation site is not a trivial issue. All possible reaction sites are considered but only the results relative to the most stable protonation sites are listed in Table 3: for DHB the most stable protonation site is the COOH group, in accordance with previous literature [22], for ATT position 1 is the most stable one (the imino nitrogen adjacent to the carbon that carries the SH group), for 4HCCA the most favorable protonation site has been found to be the nitrogen of the CN group. More precisely, in the case of DHB, protonation of both OH groups is also considered. However, the COOH group is stabilized by the hydrogen bond with the oxygen atom in *ortho* position at a distance of 1.49 Å, in accordance with what reported previously [22], with the only difference that the hydrogen bond is found to be 1.69 Å long. Protonation of the *ortho* OH group collapses to the COOH protonation, while the protonation of the *meta* OH is less stable by 25 kcal/mol. For ATT the three N atoms in positions 1, 3, and 6 are considered as reaction sites. Calculations show that the N in position 1 is the most stable protonation site followed by the 3-N and 6-N (larger than 51 kcal/mol and 200 kcal/mol, respectively, the energy difference). For 4HCCA, three protonation sites are considered: the 4-hydroxyl group, the C atom in α position forming a benzylic carbocation, and the N atom on the CN group. From the calculations, the CN is the most stable protonation site followed by the α-C and the OH (15 kcal/mol and 39 kcal/mol higher than the value found for CN). The calculated values agree with those found previously using the gas-phase bracketing method in combination with Fourier transform ion cyclotron resonance (FTICR) mass spectrometry [13] and using the kinetic method [12]. Experimental PA values for DHB are in the range 197 ÷ 204 kcal/mol and for 4HCCA in the range 183 ÷ 223 kcal/mol. In the present calculations, PAs are 201 and 205 kcal/mol for DHB and 4HCCA, respectively. However we must bear in mind that the present method has not been designed to calculate absolute PAs, so the results obtained from the comparison with the experiments must be taken *cum grano salis*.

In Table 3, GA values are also indicated, showing that the calculated value of 325 kcal/mol for DHB is in accordance with the experimental value of 318 ± 2.7 kcal/mol reported [10, 40].

Finally in Table 4, the protonation and the deprotonation enthalpies relative to the proton exchange reactions between the protonated/deprotonated matrices and the peptides are calculated, more precisely if the peptide is indicated with P and the matrix with M, we define:

$$P + MH^+ \rightarrow PH^+ + M, \Delta H_{prot} = PA_P - PA_M, \quad (4)$$

$$P + (M - H^+)^- \rightarrow (P - H^+)^- + M, \Delta H_{depr} = GA_P - GA_M. \quad (5)$$

It is interesting to observe that all peptides give negative values for ΔH_{prot} exchange energies with respect to all the matrices. This indicates that the secondary ionization process (protonation) is always thermodynamically favored. In some instances, very negative values of ΔH_{prot} are obtained (up to −78 kcal/mol in the case of hexyl-AFLDASR). In addition, the calculation suggests that being the reaction very exothermic, internal energy excess may promote unwanted peptide fragmentation resulting in a decreased ion yield for the corresponding precursor peptide ion. The deprotonation process in some instances is unfavorable, with energies up to +12 kcal/mol. As a final remark we can say that peptide protonation with respect to an ionized matrix (secondary ionization) is thermodynamically strongly favorable.

Table 3. Proton affinity (PA) and gas-phase basicity (GA) for the three matrices under investigation (kcal/mol)

Matrix	PA	GA
DHB	201	325
ATT	218	315
4-HCCA	205	332

Table 4. Peptide protonation and deprotonation enthalpies calculated with respect to the given matrices (kcal/mol)

	Matrix					
	DHB		4HCCA		ATT	
Peptide	ΔH_{prot}	ΔH_{depr}	ΔH_{prot}	ΔH_{depr}	ΔH_{prot}	ΔH_{depr}
RPPGF	−58	+2	−54	−5	−41	+12
Hexyl RPPGF	−69	—	−65	—	−52	—
AFLDASR	−65	−18	−61	−25	−48	−8
Hexyl AFLDASR	−78	—	−74	—	−61	—

Conclusions

The goal of this study is to investigate with a combination of classic MD and DFT calculations the secondary processes occurring in the gas phase between protonated/deprotonated matrices and peptides before and after esterification. We have initially validated the reliability of our computational approach by comparing our results with calculations performed using other methodologies. It is important to bear in mind that although absolute protonation and deprotonation enthalpies have to be calculated, the focus of this paper is the determination of proton transfer reaction enthalpies between peptides, native and derivatized, and protonated matrices. Considering the results, apparently the presence of $[P-H]^-$ peptide ions in the spectrum can be explained as a direct consequence of desorption of preformed ions from the solid phase by the laser [41], or due to proton exchange between matrix anions and neutral peptide in the gas-phase. In fact, if deprotonated matrix ions are expected to exist in the gas phase, secondary processes leading to formation of peptide anions are calculated to be thermodynamically favorable, at least for the AFLDASR peptide. With respect to previous computational studies [23] in which the ionization potentials of matrix-peptide clusters formed during single step ionization are calculated, our approach takes into account only the secondary processes, assuming that primary ionization of the matrix occurs in a much shorter time scale. Finally, the substantial increase in proton affinity following esterification between 11 and 13 kcal/mol suggests that the improved detection in positive mode for the ester ions is likely to be related to an increase in PA following esterification. Two hypotheses exist to explain the better MALDI response of the derivatized peptide ions: (1) an increase in PA following esterification or (2) a better incorporation into the matrix crystal caused by the higher hydrophobicity of the ester. From our results, it emerges that the rather large variations of the PA between native and derivatized peptides seems to support the first assumption. In fact, in the light of the current results, the increase in PA following esterification remains the most corroborated hypothesis in place to explain the phenomenon under study.

Acknowledgments

The authors acknowledge Shimadzu Corporation for funding this work. They are grateful for the generous INSTM grant of computer time on the IBM SP5 of CINECA (Bologna, Italy).

Appendix A Supplementary Material

Supplementary material associated with this article may be found in the online version at doi:10.1016/j.jasms.2009.03.008.

References

1. Karas, M.; Bachmann, D.; Hillenkamp, F. Influence of the Wavelenghth in High-Irradiance Ultraviolet Laser Desorption Mass Spectrometry of Organic Molecules. *Anal. Chem.* **1985,** *57,* 2935–2939.
2. Tanaka, K.; Waki, H.; Ido, Y.; Akita, S.; Yoshida, Y.; Yoshida, T. Protein and Polymer Analyses up to *m/z* 100,000 by Laser Ionization Time-of-Flight Mass Spectrometry. *Rapid Commun. Mass Spectrom.* **1988,** *2,* 151–153.
3. Zenobi, R.; Knochenmuss, R. Ion formation in MALDI Mass Spectrometry. *Mass Spectrom. Rev.* **1998,** *17,* 337–366.
4. Knochenmuss, R.; Stortelder, A.; Breuker, K.; Zenobi, R. Secondary Ion–Molecule Reactions in Matrix-Assisted Laser Desorption/Ionization. *J. Mass Spectrom.* **2000,** *35,* 1237–1245.
5. Dreisewerd, K. The Desorption Process in MALDI. *Chem. Rev.* **2003,** *103,* 395–426.
6. Knochenmuss, R.; Zenobi, R. MALDI Ionization: The Role of In-Plume Processes. *Chem. Rev.* **2003,** *103,* 441–452.
7. Knochenmuss, R. Ion Formation Mechanisms in UV-MALDI. *Analyst* **2006,** *131,* 966–986.
8. Liao, P. C.; Allison J. Ionization Processes in Matrix-Assisted Laser Desorption Ionization Mass Spectrometry: Matrix-Assisted Formation of $[M + H]^+$ vs. $[M - H]^-$ Ions of Small Peptides and Some Mechanistic Comments. *J. Mass Spectrom.* **1995,** *30,* 408–423.
9. Knochenmuss, R. A Quantitative Model of Ultraviolet Matrix-Assisted Laser Desorption/Ionization Including Analyte Ion Generation. *Anal. Chem.* **2003,** *75,* 2199–2207.
10. Harrison, A. G. The Gas-Phase Basicities and Proton Affinities of Amino Acids and Peptides. *Mass Spectrom. Rev.* **1997,** *16,* 201–217.
11. Jorgensen, T. J. D.; Bojesen, G.; Nielsen, H. R. The Proton Affinities of Seven Matrix-Assisted Laser Desorption Ionization Matrices Correlated with the Formation of Multiply-Charged Ions. *Eur. J. Mass Spectrom.* **1998,** *1,* 31–45.
12. Mirza, S. P.; Raju, N. P.; Vairamani, M. Estimation of the Proton Affinity Values of Fifteen Matrix-Assisted Laser Desorption/Ionization Matrices Under Electrospray Ionization Conditions Using the Kinetic Method. *J. Am. Soc. Mass Spectrom.* **2004,** *15,* 431–435.
13. Burton, R. D.; Watson, C. H.; Eyler, J. R.; Lang, G. L.; Powell, D. H.; Avery, M. Y. Proton Affinities of Eight Matrices Used for Matrix-Assisted Laser Desorption/Ionization. *Rapid Commun. Mass Spectrom.* **1997,** *11,* 443–446.
14. Olumee, Z.; Sadeghi, M.; Tang, X. D.; Vertes, A. Amino Acid Composition and Wavelenghth Effects in Matrix-Assisted Laser-Desorption Ionization. *Rapid Commun. Mass Spectrom.* **1995,** *9,* 744–752.
15. Krause, E.; Wenschuh, H.; Jungblut, P. R. The Dominance of Arginine-Containing Peptides in MALDI-Derived Tryptic Mass Fingerprints of Proteins. *Anal. Chem.* **1999,** *71,* 4160–4165.
16. Brancia, F. L.; Oliver, S. G.; Gaskell, S. J. Improved Matrix-Assisted Laser Desorption/Ionization Mass Spectrometric Analysis of Tryptic Hydrolysates of Proteins Following Guanidination of Lysine-Containing Peptides. *Rapid Commun. Mass Spectrom.* **2000,** *14,* 2070–2073.
17. Keough, T.; Youngquist, R. S.; Lacey, M. P. A Method for High-Sensitivity Peptide Sequencing Using Post-Source Decay Matrix-Assisted Laser Desorption Ionization Mass Spectrometry. *Proc. Natl. Acad. Sci. U.S.A.* **1999,** *96,* 7131–7136.
18. Lecchi, P.; Olson, M.; Brancia, F. L. The Role of Esterification on Detection of Protonated and Deprotonated Peptide Ions in Matrix Assisted Laser Desorption/Ionization (MALDI) Mass Spectrometry (MS). *J. Am. Soc. Mass Spectrom.* **2005,** *16,* 1269–1274.
19. Paizs, B.; Suhai, S. Fragmentation Pathways of Protonated Peptides. *Mass Spectrom. Rev.* **2004,** *24,* 508–548.
20. Bleiholder, C.; Suhai, S.; Paizs, B. Revising the Proton Affinity Scale of the Naturally Occurring α-Amino Acids. *J. Am. Soc. Mass Spectrom.* **2006,** *17,* 1275–1281.
21. Hoyau, S.; Norrman, K.; McMahon, T. B.; Ohanessian, G. A Quantitative Basis for a Scale of Na Affinities of Organic and Small Biological Molecules in the Gas Phase. *J. Am. Chem. Soc.* **1999,** *121,* 8864–8875.
22. Bourcier, S.; Hoppilliard, Y. B3LYP DFT Molecular Orbital Approach, an Efficient Method to Evaluate the Thermochemical Properties of MALDI Matrices. *Int. J. Mass Spectrom.* **2002,** *217,* 231–244.

23. Yassin, F. H.; Marynick, D. S. Computational Study of Matrix-Peptide Interactions in MALDI Mass Spectrometry: Interaction of 2,5- and 3,5-Dihydroxybenzoic Acid with the Tripeptide Valine-Proline-Leucine. *J. Phys. Chem. A* **2006,** *110,* 3820–3825.
24. Parr, R. G.; Yang, W. Density Functional Theory of Atoms and Molecules, Oxford University Press: New York, NY, **1989.**
25. Cornell, W. D.; Cieplak, P.; Bayly, C. I.; Gould, I. R.; Merz, K. M.; Ferguson, D. M.; Spellmeyer, D. C.; Fox, T.; Caldwell, J. W.; Kollman, P. A. A Second Generation Force Field for the Simulation of Proteins, Nucleic Acids, and Organic Molecules. *J. Am. Chem. Soc.* **1995,** *117,* 5179–5197.
26. Cheatham, T. E.; Cieplak, P.; Kollman, P. A. A Modified Version of the Cornell et al. Force Field with Improved Sugar Pucker Phases and Helical Repeat. *J. Biomol. Struct. Dyn.* **1999,** *16,* 845–862.
27. Becke, A. D. Density-Functional Exchange-Energy Approximation with Correct Asymptotic-Behavior. *Phys. Rev. A* **1988,** *38,* 3098–3100.
28. Lee, C. T.; Yang, W. T.; Parr, R. G. Development of the Colle-Salvetti Correlation-Energy Formula into a Functional of the Electron-Density. *Phys. Rev. B* **1988,** *37,* 785–789.
29. Singh, U. C.; Kollman, P. A. An Approach to Computing Electrostatic Charges for Molecules. *J. Comput. Chem.* **1984,** *5,* 129–145.
30. Besler, B. H.; Merz, K. M.; Kollman, P. A. Atomic Charges Derived from Semiempirical Methods. *J. Comput. Chem.* **1990,** *11,* 431–439.
31. Strittmatter, E. F.; Williams, E. R. Structures of Protonated Arginine Dimer and Bradykinin Investigated by Density Functional Theory: Further Support for Stable Gas-Phase Salt Bridges. *J. Phys. Chem. A* **2000,** *104,* 6069–6076.
32. Rodriquez, C. F.; Orlova, G.; Guo, Y.; Li, X.; Siu, C. K.; Hopkinson, A. C.; Siu, K. W. Gaseous Bradykinin and Its Singly, Doubly, and Triply Protonated Forms: a First-Principles Study. *J. Phys. Chem. B* **2006,** *110,* 7528–7537.
33. Baerends, E. J.; Ellis, D. E.; Ros, P. Self-Consistent Molecular Hartree-Fock-Slater Calculations. I. The Computational Procedure. *Chem. Phys.* **1973,** *2,* 41–51.
34. Guerra, C. F.; Snijders, J. G.; te Velde, G.; Baerends, E. J. Towards an Order-N DFT Method. *Theo. Chem. Acct.* **1998,** *99,* 391–403.
35. Vosko, S. H.; Wilk, L.; Nusair, M. Accurate Spin-Dependent Electron Liquid Correlation Energies for Local Spin-Density Calculations—A Critical Analysis. *Can. J. Phys.* **1980,** *58,* 1200–1211.
36. Perdew, J. P. Density-Functional Approximation for the Correlation-Energy of the Inhomogeneous Electron Gas. *Phys. Rev. B* **1986,** *33,* 8822–8824.
37. Bouchoux, G. Evaluation of the Protonation Thermochemistry Obtained by the Extended Kinetic Method. *J. Mass Spectrom.* **2006,** *41,* 1006–1013.
38. Brancia, F. L.; Lecchi, P. Effect of Esterification on the MALDI Response of Peptide Ions. *Proceedings of the 51st ASMS Conference on Mass Spectrometry and Allied Topics*; Montreal, Canada, June 2003.
39. Brancia, F. L.; Openshaw, M. E.; Kumashiro, S. Investigation of the Electrospray Response of Lysine-, Arginine-, and Homoarginine-Terminal Peptide Mixtures by Liquid Chromatography/Mass Spectrometry. *Rapid Commun. Mass Spectrom.* **2002,** *16,* 2255–2259.
40. Breuker, K.; Knochenmuss, R.; Zenobi, R. Gas-Phase Basicities of Deprotonated Matrix-Assisted Laser Desorption/Ionization Matrix Molecules. *Int. J. Mass Spectrom.* **1999,** *184,* 25–38.
41. Gluckmann, M.; Karas, M. Special Feature: Perspective—The Initial Ion Velocity and Its Dependence on Matrix, Analyte, and Preparation Method in Ultraviolet Matrix-Assisted Laser Desorption Ionization. *J. Mass Spectrom.* **1999,** *34,* 467–477.
42. Schnier, P. D.; Price, R. A.; Jockusch, R. A.; Williams, E. R. Blackbody Infrared Radiative Dissociation of Bradykinin and Its Analogues: Energetics, Dynamics, and Evidence for Salt-Bridge Structures in the Gas Phase. *J. Am. Chem. Soc.* **1996,** *118,* 7178–7189.